

Fig. 1. Temperature dependence of the dielectric constant  $\epsilon$  (○) and its reciprocal  $1/\epsilon$  (×) along the  $c^*$ -direction of  $\{(NH_4)_3H(SO_4)_2\}_{0.03}\{(ND_4)_3D(SO_4)_2\}_{0.97}$  at  $p=3.72$  kbar. Vertical arrows indicate the dielectric anomalies at the II-IX and IX-VI transitions. Frequency: 100 kHz.

$1/\epsilon$  along the  $c^*$ -direction of the deuterated compound at  $p=3.72$  kbar. As shown by the arrows, two anomalies are seen around the II  $\rightarrow$  VI transition region. These anomalies indicate that there is an intermediate phase in a narrow temperature region between the room temperature phase of II and the ferroelectric VI phase. The intermediate phase is denoted as Phase IX. Figure 2 indicates the temperature dependence of the inverse of the dielectric constant  $1/\epsilon$  at pressures higher than 6 kbar. A clear break is seen for each curve as indicated

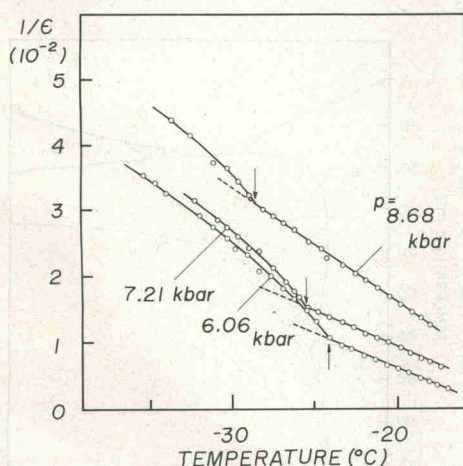


Fig. 2. Temperature dependence of the reciprocal of the dielectric constant  $1/\epsilon$  along the  $c^*$ -direction of  $\{(NH_4)_3H(SO_4)_2\}_{0.03}\{(ND_4)_3D(SO_4)_2\}_{0.97}$  at different hydrostatic pressures. Vertical arrows indicate the anomalies at the VIII-VI transition. Frequency: 100 kHz.

by an arrow. The dielectric anomaly corresponds to a phase transition from the room temperature phase of II to a new intermediate phase which is denoted as Phase VIII. The pressure-induced phases of VIII and IX were not noticed in our preliminary work.<sup>6)</sup>

From the results of dielectric constant measurements, we can obtain the pressure-temperature phase diagrams for different concentration  $x$ . Figures 3~8 show the  $p$ - $T$  phase diagrams for compounds with  $x=0, 0.14, 0.40, 0.60, 0.79,$  and  $0.97$ , respectively. The phase diagram of the normal compound shown in Fig. 3 was the one reported previously.<sup>3)</sup> As the deuterium concentration increases the two pressure-induced ferroelectric phases VI and VII appear in lower pressure region. The intermediate phase IX can be seen in the pressure region studied for the compounds with  $x \geq 0.60$ .

In the normal compound the II-III phase boundary was not represented by a linear relation, but it was approximated by a quadratic form of  $\Theta_{II-III} = T_{II-III}^0 + Kp + \gamma p^2$ .<sup>9)</sup> We estimated the parameters  $T_{II-III}^0$ ,  $K$ , and  $\gamma$  as functions of  $x$  from the phase diagrams. The results are shown in Fig. 9. The II-III transition temperature  $T_{II-III}^0$  at 0 kbar and the initial pressure slope  $K$  vary with concentration  $x$  very slightly. On the other hand, the parameter

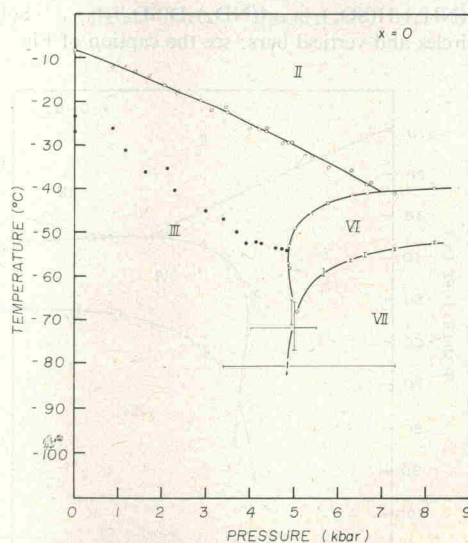


Fig. 3. Pressure-temperature phase diagram of  $(NH_4)_3H(SO_4)_2$ .<sup>3)</sup> Solid circles show the position of the broad dielectric constant peak at constant-pressure runs. Short bars indicate temperature (or pressure) hysteresis of the first order transitions.

$\gamma$  seems to change its sign as  $x$  varies from 0 to 0.97.

Figure 10 shows the pressure dependence of the inverse of the maximum value of the dielectric constant at the diffuse peak in Phase III for different  $x$ . The relation between  $1/\epsilon_{\max}$  and pressure  $p$  is linear for each compound, that is, a Curie-Weiss like relation  $1/\epsilon_{\max} = C^*(p_0 - p)$  is held. The relations between  $1/\epsilon_{\max}$  against  $p$  for various deuterium concentrations  $x$  are almost parallel. Therefore the constant  $C^*$  is practically unchanged as deuterium con-

centration varies. The critical pressure  $p_c$  above which the ferroelectric VI phase appears is shown in Fig. 11 as a function of  $x$ . The experimental point corresponding to  $p=0$  is determined from the  $x$ - $T$  phase diagram at atmospheric pressure measured previously.<sup>4)</sup> The critical pressure  $p_c$  varies nearly linearly with the deuterium concentration  $x$  in the region  $x \leq 0.5$ . As the deuterium concentration further increases a deviation from the linear relation becomes progressively large. The

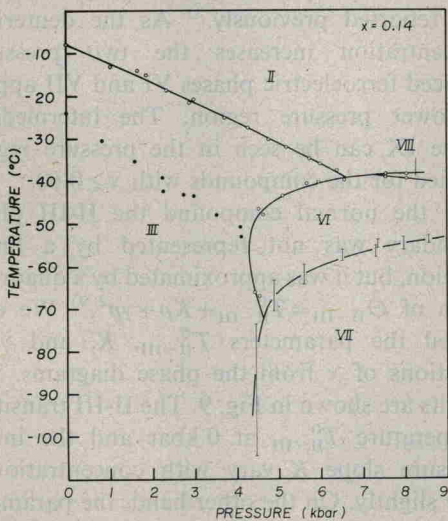


Fig. 4. Pressure-temperature phase diagram of  $\{(\text{NH}_4)_3\text{H}(\text{SO}_4)_2\}_{0.86}\{(\text{ND}_4)_3\text{D}(\text{SO}_4)_2\}_{0.14}$ . Solid circles and vertical bars: see the caption of Fig. 3.

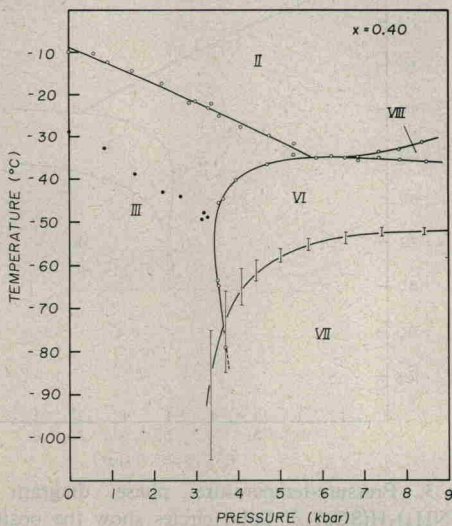


Fig. 5. Pressure-temperature phase diagram of  $\{(\text{NH}_4)_3\text{H}(\text{SO}_4)_2\}_{0.60}\{(\text{ND}_4)_3\text{D}(\text{SO}_4)_2\}_{0.40}$ . Solid circles and vertical bars: see the caption of Fig. 3.

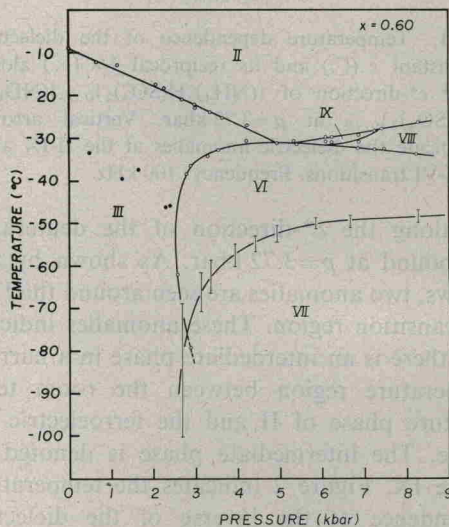


Fig. 6. Pressure-temperature phase diagram of  $\{(\text{NH}_4)_3\text{H}(\text{SO}_4)_2\}_{0.40}\{(\text{ND}_4)_3\text{D}(\text{SO}_4)_2\}_{0.60}$ . Solid circles and vertical bars: see the caption of Fig. 3.

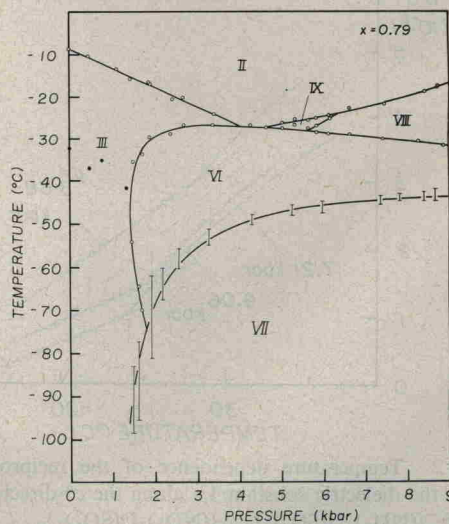


Fig. 7. Pressure-temperature phase diagram of  $\{(\text{NH}_4)_3\text{H}(\text{SO}_4)_2\}_{0.21}\{(\text{ND}_4)_3\text{D}(\text{SO}_4)_2\}_{0.79}$ . Solid circles and vertical bars: see the caption of Fig. 3.